Unconstrained Simultaneous Scheme to Fully Couple Reconstruction and Registration for Digital Breast Tomosynthesis: A Feasible Study

Guang Yang[†1], John H. Hipwell[1], David J. Hawkes[1], and Simon R. Arridge[1]

Centre for Medical Image Computing, Department of Computer Science and Medical Physics, University College London (UCL), London, WC1E 6BT, UK

Abstract. Digital breast tomosynthesis (DBT) provides a pseudo-3D reconstruction which addresses the limitation of superimposition of dense fibro-glandular tissue associated with conventional mammography. Registration of temporal DBT volumes searches for the optimum deformation to transform two observed images of the same object into a common reference frame. This aligns the two images via minimising an objective function that calculates the similarity between the two datasets.

In this paper, we present a novel algorithm which combines reconstruction of a pair of temporal DBT acquisitions with their simultaneous registration. We approach this nonlinear inverse problem using a generic unconstrained optimisation scheme. To evaluate the performance of our method we use 2D and 3D software phantoms and demonstrate that this simultaneous approach has comparable results to performing these tasks sequentially or iteratively w.r.t both the reconstruction fidelity and the registration accuracy.

1 Introduction

DBT is an X-ray modality using a small number of low dose X-ray images, which are acquired over a limited angle and reconstructed into a 3D volume. Although reconstructed 3D DBT images possess a high in-plane resolution, they exhibit a lower out-of-plane resolution [1]. The premise is that this coarse depth resolution is sufficient to alleviate some of the problems of overlapping tissue structures that degrades the sensitivity and specificity of cancer detection and characterisation using conventional mammography. One significant aspect of DBT is the performance of the reconstruction algorithms, which have been extensively investigated over the last decade. Comprehensive reviews on the comparison of various approaches have been published by Dobbins III, Godfrey [2] and Zhang et al. [3]. A recent investigation by Candès, Romberg and Tao [4] into compressed sensing, indicates that it is possible to recover the original signal exactly, using a linear measurement model with incomplete data. This theoretical derivation is applicable to DBT reconstructions which are computed given incomplete forward projections. Therefore, mathematically, we can solve the DBT reconstruction

[†]Contact Email: {g.yang, s.arridge}@cs.ucl.ac.uk, {j.hipwell, d.hawkes}@ucl.ac.uk. This work has been funded by DTI Project Digital Breast Tomosynthesis TP/7/SEN/6/1/M1577G.

ISBN: 978-87-981270-9-3

problem perfectly, with a limited-angle set of projections, given judicious choice of appropriate constraints such as regularisation.

Early breast cancer detection requires the recognition of subtle pathological changes, such as those due to tumour growth, over time. These abnormal changes and deformations of the breast tissue must be distinguished from normal deformations caused by differences in breast position, compression and other imaging acquisition parameters between the two time-points. In the high throughput breast screening context [5], the additional depth information provided by DBT must be integrated into the workflow in a way that enhances performance but does not increase the workload of the clinicians involved. In this respect, image registration could play an important role in eliminating differences between the temporal DBT datasets due to patient position, allowing the observer to focus on identifying those changes which might be indicative of disease.

Previous work on DBT image registration is limited. Sinha et al. [6] describe application of a thin-plate spline registration of corresponding manually selected control points, using mutual information as the cost function. They applied this method to seven subjects' datasets which were acquired between one year and a few minutes apart and estimate the registration accuracy to be 1.8mm $\pm$1.4. Zhang and Brady [7] describe a method for feature point extraction and use the resulting landmarks to drive a polyaffine registration of a single pair of DBT datasets.

Whilst combined registration and reconstruction algorithms have been applied to other modalities (*e.g.* PET and MRI), little has been published on applying these techniques to DBT. Yang et al. [8] [9] proposed an iterative method, which *partially coupled* the two tasks by alternating between optimising image intensity and deformation parameters to obtain a reduced cost functional. Rather than registering the images after reconstruction or partially coupling them, we advocate a method which combines the two tasks simultaneously (*fully coupled*) in order to avoid the assumptions of missing data being equal to zero (implicit in algorithms such as FBP). The aim of this work is to show that reconstruction and registration are not independent, and that combining these tasks will enhance the performance of each process as a result.

2 Methods

Based on the motivation and hypothesis above, we have developed an algorithm, which outputs one unified result for the reconstruction and registration. However, the introduction of registration introduces nonlinearity of the transformation parameters making solution of the inverse problem more complex. Although the following experiments were performed using an affine transformation and sum of squared differences, as the cost function, other higher order non-rigid transformations and alternative similarity measurements can naturally be substituted into our simultaneous framework. Before presenting our simultaneous method, we first describe the *conventional method* of performing registration after both volumes have been successfully reconstructed. Then we paraphrase the *itera-*

ISBN: 978-87-981270-9-3

tive method proposed by Yang et al. [8] [9], and subsequently we propose our *simultaneous algorithm*.

2.1 Conventional Sequential Method

A 3D object, $\boldsymbol{x} \in \Re^{N_3}$, two sets of (in our case simulated) temporal data, $\boldsymbol{y_1}$, $\boldsymbol{y_2} \in \Re^{\kappa \cdot N_2}$, (acquired using limited angle DBT geometry with $\kappa = 11$ projections covering $\pm 25^{\circ}$), the parametric transformation matrix, $R_{\boldsymbol{\zeta_p}}$, and the system matrix, $A \in \Re^{\kappa \cdot N_2 \times N_3} : \Re^{N_3} \mapsto \Re^{N_2}$, can be related via

$$\boldsymbol{y_1} = A\boldsymbol{x}, \tag{1}$$

and

$$\boldsymbol{y_2} = A\boldsymbol{x^*} = AR_{\boldsymbol{\zeta_p}}\boldsymbol{x}. \tag{2}$$

A describes the forward model to mimic the X-ray attenuation, scattering or absorption properties. The reconstruction of equations 1 and 2 can be solved by minimising

$$\boldsymbol{x_1}^{\dagger} = \arg\min_{\boldsymbol{x_1}} \left(\Phi_{Rec1} = \frac{1}{2}\left\|A\boldsymbol{x_1} - \boldsymbol{y_1}\right\|_2^2 \right); \tag{3}$$

$$\boldsymbol{x_2}^{\dagger} = \arg\min_{\boldsymbol{x_2}} \left(\Phi_{Rec2} = \frac{1}{2}\left\|A\boldsymbol{x_2} - \boldsymbol{y_2}\right\|_2^2 \right). \tag{4}$$

Following reconstruction, volumes $\boldsymbol{x_1}^{\dagger}$ and $\boldsymbol{x_2}^{\dagger}$, i.e. the fixed and moving images, are registered w.r.t the registration parameters $\boldsymbol{\zeta_p}$:

$$\boldsymbol{\zeta_p}^{\dagger} = \arg\min_{\boldsymbol{\zeta_p}} \left(\Phi_{Reg} = \frac{1}{2}\left\|R_{\boldsymbol{\zeta_p}}\boldsymbol{x_2}^{\dagger} - \boldsymbol{x_1}^{\dagger}\right\|_2^2 \right). \tag{5}$$

2.2 Partially Coupled Iterative Method

According to the previous investigations of the partially coupled iterative method [8, 9], the equations 1 and 2 can be solved by alternating an incomplete optimisation, i.e. n iterations, of the reconstructed volumes $\boldsymbol{x_1}$ and $\boldsymbol{x_2}$

$$\boldsymbol{x_1}^{\ddagger} = \arg\min_{\boldsymbol{x_1}} \left(\Phi_{Rec1} = \frac{1}{2}\left\|A\boldsymbol{x_1} - \boldsymbol{y_1}\right\|_2^2 \right) \tag{6}$$

$$\boldsymbol{x_2}^{\ddagger} = \arg\min_{\boldsymbol{x_2}} \left(\Phi_{Rec2} = \frac{1}{2}\left\|A\boldsymbol{x_2} - \boldsymbol{y_2}\right\|_2^2 \right) \tag{7}$$

with registration of the current estimates $\boldsymbol{x_1}^{\ddagger}$ and $\boldsymbol{x_2}^{\ddagger}$ w.r.t the registration parameters $\boldsymbol{\zeta_p}$:

$$\boldsymbol{\zeta_p}^{\ddagger} = \arg\min_{\boldsymbol{\zeta_p}} \left(\Phi_{Reg} = \frac{1}{2}\left\|R_{\boldsymbol{\zeta_p}}\boldsymbol{x_2}^{\ddagger} - \boldsymbol{x_1}^{\ddagger}\right\|_2^2 \right). \tag{8}$$

This method is summarised in Algorithm 1. The reconstruction-registration loop repeats m times and outputs $\boldsymbol{x_1} = \boldsymbol{x_1}^{\ddagger}$, $\boldsymbol{x_2} = \boldsymbol{x_2}^{\ddagger}$ and $R_{\boldsymbol{\zeta_p}}\boldsymbol{x_2}^{\ddagger}$

ISBN: 978-87-981270-9-3

Algorithm 1: Partially Coupled Iterative Reconstruction and Registration

Input: $\boldsymbol{y_1},\ \boldsymbol{y_2}$.
Output: $\boldsymbol{x_1},\ \boldsymbol{x_2},\ R_{\zeta_p}\boldsymbol{x_2}$.

begin
  % Initialization of $\boldsymbol{x_1}$ and $\boldsymbol{x_2}$
  ${\boldsymbol{x_1}}^{0,0} := 0$; ${\boldsymbol{x_2}}^{0,0} := 0$; ${\boldsymbol{\zeta_p}}^{0} := 0$;

  % Outer loop for the registration
  for $(i = 0;\ i < m;\ i++)$ **do**
    % Inner loop for the reconstruction
    for $(j = 0;\ j < n;\ j++)$ **do**
      % $\Psi_{\boldsymbol{x}}$ is the analytical gradient of the $\boldsymbol{x}$
      % for the CG or L-BFGS solver
      ${\Psi_{\boldsymbol{x_1}}}^{i,j} := A^T(A{\boldsymbol{x_1}}^{i,j} - \boldsymbol{y_1})$;
      ${\Psi_{\boldsymbol{x_2}}}^{i,j} := A^T(A{\boldsymbol{x_2}}^{i,j} - \boldsymbol{y_2})$;
      ${\boldsymbol{x_1}}^{i,j+1} := {\boldsymbol{x_1}}^{i,j} + (A^TA)^{-1}{\Psi_{\boldsymbol{x_1}}}^{i,j}$;
      ${\boldsymbol{x_2}}^{i,j+1} := {\boldsymbol{x_2}}^{i,j} + (A^TA)^{-1}{\Psi_{\boldsymbol{x_2}}}^{i,j}$;
    % Run a simple hill-climbing optimisation
    ${\boldsymbol{\zeta_p}}^{i+1} := \arg\min_{{\zeta_p}^i} \frac{1}{2}\|R_{{\zeta_p}^i}\boldsymbol{x_2}^{\boldsymbol{i,j+1}} - \boldsymbol{x_1}^{\boldsymbol{i,j+1}}\|_2^2$;
    ${\boldsymbol{x_1}}^{i+1,j+1} := R_{{\boldsymbol{\zeta_p}}^{i+1}}\boldsymbol{x_2}^{\boldsymbol{i,j+1}}$;
    ${\boldsymbol{x_2}}^{i+1,j+1} := \boldsymbol{x_2}^{\boldsymbol{i,j+1}}$;

  % Output $\boldsymbol{x_1}$, $\boldsymbol{x_2}$, and $R_{\zeta_p}\boldsymbol{x_2}$
  $\boldsymbol{x_1} := \boldsymbol{x_1}^{\boldsymbol{i,j+1}}$;
  $\boldsymbol{x_2} := {\boldsymbol{x_2}}^{i+1,j+1}$;
  $R_{\zeta_p}\boldsymbol{x_2} := {\boldsymbol{x_1}}^{i+1,j+1} := R_{{\boldsymbol{\zeta_p}}^{i+1}}\boldsymbol{x_2}^{\boldsymbol{i,j+1}}$.
end

2.3 Our Simultaneous Method

The ultimate goal of our simultaneous method is to obtain an enhanced reconstruction and more accurate registration of both volumes, to aid the reading process and improve the detection of malignant tissue change. Therefore, we propose a simultaneous method using an *unconstrained* reconstruction and registration framework expressed mathematically as in Algorithm 2. Firstly, the objective function is described as

$$\min_{\boldsymbol{x},\boldsymbol{\zeta_p}\in\Re^n} \Phi_{RR} = \frac{1}{2}\Big(||A\boldsymbol{x} - \boldsymbol{y_1}||^2 + ||AR_{\boldsymbol{\zeta_p}}\boldsymbol{x} - \boldsymbol{y_2}||^2\Big), \tag{9}$$

in which, $\boldsymbol{y_1}$ and $\boldsymbol{y_2}$ are the two input X-ray acquisitions, and $\boldsymbol{x}$ denotes the unknown estimated volume. We combine the two sets of reconstructions $||A\boldsymbol{x} - \boldsymbol{y_1}||^2$ and $||AR_{\boldsymbol{\zeta_p}}\boldsymbol{x} - \boldsymbol{y_2}||^2$ with an affine registration with 12 degrees of freedom $\boldsymbol{\zeta_p}, (p = 1, 2, \ldots, 12)$, which globally describes the translation, scaling, rotation and shearing in 3D, or $\boldsymbol{\zeta_p}, (p = 1, 2, \ldots, 6)$ denotes 6 degrees of freedom in 2D.

A minimiser $\boldsymbol{x}, \boldsymbol{\zeta_p} \in \Re^n$ of Φ_{RR} is characterised by the necessary condition that the partial derivative w.r.t $\boldsymbol{x}$ and $\boldsymbol{\zeta_p}$ equals 0, denoted by $\nabla\Phi_{RR} = 0$. The partial derivative w.r.t $\boldsymbol{x}$ is straightforward, and is given by

$$g_{\boldsymbol{x}} = \frac{\partial\Phi_{RR}}{\partial\boldsymbol{x}} = A^T(A\boldsymbol{x} - \boldsymbol{y_1}) + R_{\boldsymbol{\zeta_p}}^T A^T(AR_{\boldsymbol{\zeta_p}}\boldsymbol{x} - \boldsymbol{y_2}), \tag{10}$$

ISBN: 978-87-981270-9-3

in which, $\frac{\partial \Phi_{RR}}{\partial \boldsymbol{x}}$ is the gradient. Similarly the Hessian can be expressed as

$$H_{\boldsymbol{x}} = \frac{\partial \Phi_{RR}}{\partial^2 \boldsymbol{x}} = A^T A + R_{\boldsymbol{\zeta_p}}^T A^T A R_{\boldsymbol{\zeta_p}}. \tag{11}$$

To derive the partial derivative w.r.t $\boldsymbol{\zeta_p}$, we apply a small perturbation to the objective function,

$$\Phi_{RR}\Big(\boldsymbol{x}, \boldsymbol{\zeta_p} + \Delta\boldsymbol{\zeta_p}\Big) = \frac{1}{2}\Big(||A\boldsymbol{x} - \boldsymbol{y_1}||^2 + ||AR_{\boldsymbol{\zeta_p}+\Delta\boldsymbol{\zeta_p}}\boldsymbol{x} - \boldsymbol{y_2}||^2\Big) \tag{12}$$

$$\approx \frac{1}{2}\Big(||A\boldsymbol{x} - \boldsymbol{y_1}||^2 + ||AR_{\boldsymbol{\zeta_p}}\boldsymbol{x} + A\frac{\partial R_{\boldsymbol{\zeta_p}}}{\partial \boldsymbol{\zeta_p}}\boldsymbol{x}\Delta\boldsymbol{\zeta_p} - \boldsymbol{y_2}||^2\Big). \tag{13}$$

By taking the derivative w.r.t $\Delta\boldsymbol{\zeta_p}$, we obtain that

$$\Big(A\frac{\partial R_{\boldsymbol{\zeta_p}}}{\partial \boldsymbol{\zeta_p}}\boldsymbol{x}\Big)^T\Big(AR_{\boldsymbol{\zeta_p}}\boldsymbol{x} + A\frac{\partial R_{\boldsymbol{\zeta_p}}}{\partial \boldsymbol{\zeta_p}}\boldsymbol{x}\Delta\boldsymbol{\zeta_p} - \boldsymbol{y_2}\Big) = 0; \tag{14}$$

and if $g_{\boldsymbol{\zeta_p}}$ and $H_{\boldsymbol{\zeta_p}}$ denote the gradient and Hessian respectively then we have,

$$\Big(A\frac{\partial R_{\boldsymbol{\zeta_p}}}{\partial \boldsymbol{\zeta_p}}\boldsymbol{x}\Big)^T\Big(A\frac{\partial R_{\boldsymbol{\zeta_p}}}{\partial \boldsymbol{\zeta_p}}\boldsymbol{x}\Big)\Delta\boldsymbol{\zeta_p} = -\Big(A\frac{\partial R_{\boldsymbol{\zeta_p}}}{\partial \boldsymbol{\zeta_p}}\boldsymbol{x}\Big)^T\Big(AR_{\boldsymbol{\zeta_p}}\boldsymbol{x} - \boldsymbol{y_2}\Big), \tag{15}$$

and therefore,

$$\Delta\boldsymbol{\zeta_p} = -\left[\Big(A\frac{\partial R_{\boldsymbol{\zeta_p}}}{\partial \boldsymbol{\zeta_p}}\boldsymbol{x}\Big)^T\Big(A\frac{\partial R_{\boldsymbol{\zeta_p}}}{\partial \boldsymbol{\zeta_p}}\boldsymbol{x}\Big) + \lambda I\right]^{-1}\Big(A\frac{\partial R_{\boldsymbol{\zeta_p}}}{\partial \boldsymbol{\zeta_p}}\boldsymbol{x}\Big)^T\Big(AR_{\boldsymbol{\zeta_p}}\boldsymbol{x} - \boldsymbol{y_2}\Big), \tag{16}$$

in which,

$$g_{\boldsymbol{\zeta_p}} = \frac{\partial \Phi_{RR}}{\partial \boldsymbol{\zeta_p}} = \Big(A\frac{\partial R_{\boldsymbol{\zeta_p}}}{\partial \boldsymbol{\zeta_p}}\boldsymbol{x}\Big)^T\Big(AR_{\boldsymbol{\zeta_p}}\boldsymbol{x} - \boldsymbol{y_2}\Big) = \Big(AR'_{\boldsymbol{\zeta_p}}\boldsymbol{x}\Big)^T\Big(AR_{\boldsymbol{\zeta_p}}\boldsymbol{x} - \boldsymbol{y_2}\Big), \tag{17}$$

and

$$H_{\boldsymbol{\zeta_p}} = \Big(A\frac{\partial R_{\boldsymbol{\zeta_p}}}{\partial \boldsymbol{\zeta_p}}\boldsymbol{x}\Big)^T\Big(A\frac{\partial R_{\boldsymbol{\zeta_p}}}{\partial \boldsymbol{\zeta_p}}\boldsymbol{x}\Big) = \Big(AR'_{\boldsymbol{\zeta_p}}\boldsymbol{x}\Big)^T\Big(AR'_{\boldsymbol{\zeta_p}}\boldsymbol{x}\Big). \tag{18}$$

In order to apply a generic non-linear conjugate gradient optimiser, we extract the gradients of the objective function w.r.t $\boldsymbol{x}$ and $\boldsymbol{\zeta_p}$ below

$$\nabla\Phi_{RR} = \begin{pmatrix} \frac{\partial \Phi_{RR}}{\partial \boldsymbol{x}} \\ \frac{\partial \Phi_{RR}}{\partial \boldsymbol{\zeta_p}} \end{pmatrix} = \begin{pmatrix} A^T(A\boldsymbol{x} - \boldsymbol{y_1}) + R_{\boldsymbol{\zeta_p}}^T A^T(AR_{\boldsymbol{\zeta_p}}\boldsymbol{x} - \boldsymbol{y_2}) \\ \Big(AR'_{\boldsymbol{\zeta_p}}\boldsymbol{x}\Big)^T\Big(AR_{\boldsymbol{\zeta_p}}\boldsymbol{x} - \boldsymbol{y_2}\Big) \end{pmatrix}. \tag{19}$$

3 Experiments and Results

3.1 2D Shepp-Logan Phantom

For a first test, a 2D Shepp-Logan phantom is used to demonstrate the feasibility and performance of our new simultaneous approach. The fixed and moving images are of size 64^2 pixel, with a simulated affine transformation between them.

ISBN: 978-87-981270-9-3

We test with 10 different sets of deformations, which contain 6 affine parameters p_1 to p_6 as seen in Table 1, and we calculate the mean error and standard deviation between the recovered parameters and the ground truth. Fig. 1 shows the result of the test case number 5 using our simultaneous method.

Algorithm 2: Simultaneous Reconstruction and Registration

Input: $\boldsymbol{y_1}$, $\boldsymbol{y_2}$.
Output: $\boldsymbol{x}$, $\boldsymbol{\zeta_p}$.

begin
  % Initialization of $\boldsymbol{x}$ and $\boldsymbol{\zeta_p}$
  $\boldsymbol{x}^0 := 0$; $\boldsymbol{\zeta_p}^0 := 0$;

  % Simultaneous registration and reconstruction
  for $(i = 0;\ i < m;\ i++)$ **do**
    % $\Psi_{\boldsymbol{x}}$ and $\Psi_{\boldsymbol{\zeta_p}}$ are the analytical gradients
    % of the $\boldsymbol{x}$ and $\boldsymbol{\zeta_p}$ for the CG or L-BFGS solver

    $\Psi_{\boldsymbol{x}^i 1} := A^T(A\boldsymbol{x}^i - \boldsymbol{y_1})$;
    $\Psi_{\boldsymbol{x}^i 2} := R^T_{\boldsymbol{\zeta_p}} A^T(AR_{\boldsymbol{\zeta_p}}\boldsymbol{x}^i - \boldsymbol{y_2})$;
    $\Psi_{\boldsymbol{x}^i} := \Psi_{\boldsymbol{x}^i 1} + \Psi_{\boldsymbol{x}^i 2}$;

    $\Psi_{\boldsymbol{\zeta_p}^i} := (AR'_{\boldsymbol{\zeta_p}}\boldsymbol{x}^i)^T(AR_{\boldsymbol{\zeta_p}}\boldsymbol{x}^i - \boldsymbol{y_2})$;

    $\boldsymbol{x}^{i+1} := \boldsymbol{x}^i + (A^TA)^{-1}\Psi_{\boldsymbol{x}^i 1} + (A^TR^T_{\boldsymbol{\zeta_p}}R_{\boldsymbol{\zeta_p}}A)^{-1}\Psi_{\boldsymbol{x}^i 2}$;
    $\boldsymbol{\zeta_p}^{i+1} := \boldsymbol{\zeta_p}^i + (x^TA^TAx)^{-1}\Psi_{\boldsymbol{\zeta_p}^i}$;

  % Output the $\boldsymbol{x}$ and $\boldsymbol{\zeta_p}$
  $\boldsymbol{x} := \boldsymbol{x}^{i+1}$;
  $\boldsymbol{\zeta_p} := \boldsymbol{\zeta_p}^{i+1}$.
end

Table 1. Deformation parameters scenarios for 2D experiments. Column 2-4: Ground truth; Column 5: Initial guess; Column 6-8: Recovered parameters; Column 9: Mean error & standard deviation of 10 tests. Only the results of test no. 1, 5 and 8 are shown.

	G1	G5	G8	Initial	R1	R5	R8	Mean Error and S.D.
p_1	1.0677	1.1885	0.7794	1	1.0791	1.1872	0.9132	0.1287±0.1102
p_2	0.2796	0.1843	-0.4500	0	0.2482	0.1841	-0.2650	0.2157±0.2388
$p_3(t_x)$	2.0000	2.0000	3.0000	0	1.9753	1.9890	2.8537	0.1847±0.2114
p_4	-0.0480	0.1694	0.4779	0	-0.0057	0.1680	0.1068	0.3140±0.2278
p_5	0.9054	0.8179	0.6478	1	0.9031	0.8173	1.1935	0.4062±0.5178
$p_6(t_y)$	-1.0000	-4.0000	-1.0000	0	-1.0502	-3.9546	-0.8106	0.8050±1.1044

3.2 3D Toroid Phantom (Comparing outputs of the three methods)

In this second experiment we compare the performance of (a) the *sequential* reconstruction and registration, in which $n = 100$ iterations of the reconstruction of projection images, $\boldsymbol{y_1}$ and $\boldsymbol{y_2}$, are followed by a single registration of the reconstructed volumes $\boldsymbol{x_1}$ and $\boldsymbol{x_2}$ ($m = 1$); (b) the *partially coupled iterative* approach, in which $n = 10$ iterations of the reconstruction are followed by a registration and the process repeated $m = 10$ times and (c) our *simultaneous* method. A $70 \times 70 \times 70\text{mm}^3$ 3D toroid phantom image (resolution 1mm) is created for this purpose. Fig. 2 shows the comparison results using these three different methods.

ISBN: 978-87-981270-9-3

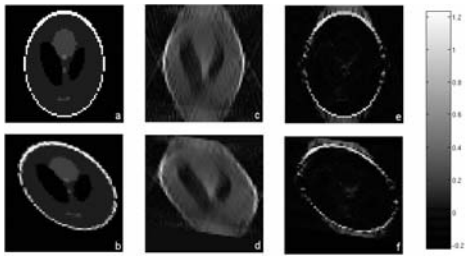

Fig. 1. *Column 1-3: The fixed image (a) and the moving image (b); the result of the simultaneous method (c), and transformation of the moving image using the recovered parameters (d); Error image (e) by subtracting (c) from (a), and error image (f) by subtracting (d) from (b).*

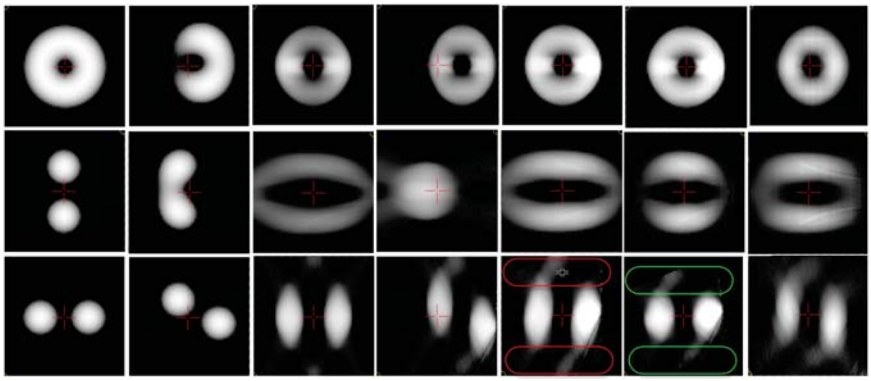

Fig. 2. *Column 1-4: Original test volume (fixed image); Its affine transformations (moving image); Reconstruction of the fixed image without registration; Reconstruction of the moving image without registration; Column 5-7: Sequential method result (transformed moving image reconstruction); Iterative method result (transformed moving image reconstruction); Our simultaneous method result (no cutting-off artefacts as shown in the colored boxes).*

4 Discussion

We have found for the first time to our knowledge that the simultaneous reconstruction and registration of DBT datasets using a generic optimisation framework is feasible. The approach jointly considers the registration and reconstruction components of the breast cancer CAD problem, and is capable of recovering both the deformation parameters, and an enhanced, reconstructed image. The performance of the new approach is demonstrated using a numerical phantom in 2D followed by a simple 3D test case. The 2D result is shown in Fig. 1, and indicates that significant reconstruction artifacts are still present. We attribute this to the fact that the unconstrained optimisation is a naïve approach, and could be improved by the addition of regularization and nonnegativity constraints.

ISBN: 978-87-981270-9-3

However, the results in Table 1 demonstrate that we have obtained reasonable recovery of the deformation parameters. These parameters are initialised using an identical transformation, in which, p_3 and p_6 are the translations t_x and t_y along each 2D direction. The mean error in t_y is relatively large because in test case no. 10 we give a large translation which translates the moving image outside of the field of view. Furthermore, the 3D test results in Fig. 2 also show that our simultaneous method is promising, and the result of our approach is compact and there is no cutting-off artefacts) when compared to the other two methods.

5 Conclusion and Perspectives

In this paper, we have presented a novel simultaneous method to fully couple reconstruction and registration for DBT, which is inspired by the motivation of detecting changes between the two sets of temporal data. SSD is employed as the registration metric, which formulates the cost criterion by the comparison between the volume estimation x and the original two sets of acquisitions y_1 and y_2. From the results on the 3D toroidal phantom images, this approach is found to reduce the misregistration artifacts with comparable reconstruction fidelity when compared to the sequential or iterative methods. There are numerous points to explore in future work. First, we would like to apply GPU acceleration for some components of our implementation, e.g. forward and backward projectors. Second, we also intend to extend the registration to incorporate non-rigid transformations. Finally, we would like to perform experiments on real DBT data, and tackle the large data size problem using multi-scale and multi-resolution techniques.

References

[1] Niklason, L.T., et al.: *Digital Tomosynthesis in Breast Imaging.* Radiology, vol. 205, 399–406 (1997)
[2] Dobbins III, J.T. and Godfrey, D.J.: *Digital X-ray Tomosynthesis: Current State of the Art and Clinical Potential.* Phys. in Med. and Bio., vol. 48, R65–R106 (2003)
[3] Zhang, Y., et al.: *A Comparative Study of Limited-angle Cone-beam Reconstruction Methods for Breast Tomosynthesis.* Medical physics, vol. 33, 3781–3795 (2006)
[4] Candès, E., Romberg, J., and Tao, T.: *Robust Uncertainty Principles: Exact Signal Reconstruction from Highly Incomplete Frequency Information.* IEEE Transactions on Information Theory, vol. 52, 489–509, (2006)
[5] Cancer Research UK: *Breast Screening in the UK: A Brief History.*
[6] Sinha, S.P., et al.: *Image Registration for Detection and Quantification of Change on Digital Tomosynthesis Mammographic Volumes.* American Journal of Roentgenology, vol. 192(2), 384–387 (2009)
[7] Zhang, W.W. and Brady, M.: *Feature Point Detection for Non-rigid Registration of Digital Breast Tomosynthesis Images.* IWDM'10, vol. 6136. LNCS, 296–303 (2010)
[8] Yang, G., et al.: *Combined Reconstruction and Registration of Digital Breast Tomosynthesis.* IWDM'10, vol. 6136. LNCS, 760–768 (2010)
[9] Yang, G., et al.: *Combined Reconstruction and Registration of Digital Breast Tomosynthesis: Sequential Method versus Iterative Method.* MIUA, 27:1–5 (2010)

ISBN: 978-87-981270-9-3